Optimization of an Electric Vehicle Traction Motor with a PM Flux Intensifying Stator and a Reluctance Outer Rotor

Oluwaseun A. Badewa, Ali Mohammadi, Donovin D. Lewis, Dan M. Ionel,
Somasundaram Essakiappan[1], and Madhav Manjrekar[1]
SPARK Laboratory, ECE Department, University of Kentucky, Lexington, KY, USA
[1]QM Power, Inc., Kansas City, MO, USA
o.badewa@uky.edu, alimohammadi@uky.edu, donovin.lewis@uky.edu, dan.ionel@ieee.org,
somasundaram@qmpower.com, mmanjrekar@qmpower.com

***Abstract*—This paper proposes a novel electric motor concept using stator-embedded phase coils and permanent magnets (PM). A unique pattern of phase coil placement in separate slots using concentrated windings is employed. High flux intensification is achieved using low remanence and non-rare-earth permanent magnets in a spoke-type field arrangement. The exterior rotor has no active electromagnetic component thereby achieving a simple reluctance type configuration. The principle of operation is based on the concept of virtual work with closed-form analytical airgap flux density distributions. Preliminary parametric design studies followed by large scale multi-objective optimization were carried out using electromagnetic FEA to study the geometric impacts of the proposed design as well as the best trade-off between torque, total loss, torque ripple and power factor. Comparative metrics including indices for flux concentration, goodness of excitation, machine goodness, and torque per weight (TRW) indicate competitive performance with PM synchronous designs employing expensive and critical supply rare-earth PMs as well as other state-of-the art high power density traction motors. The proposed novel design considers a 10in outer rotor diameter with a target torque of 370Nm at a base speed of 3,000rpm. The efficiency map of the proposed design also provides insight into its performance at constant torque and constant power regions within the considered torque-speed envelope.**

***Index Terms*—Electric vehicle, electric machine, FEA, spoke permanent magnet, flux-intensifying topology, PM synchronous**

I. Introduction

In recent years, the evolution of transportation towards electrification has gained traction due to significantly increased energy efficiency, the potential for greatly reduced emissions, and to build long-term sustainability [1]. The sustainable development of electric vehicle (EV) components for wide-scale deployment is greatly impacted by the volumetric, gravimetric and economic limitations of energy storage which leads to limited driving range otherwise known as range anxiety. Improvements to vehicle propulsion, one of the major power consumers in EVs, in efficiency and power density aids in these efforts by being able to go farther with the same amount of energy and reducing traction-related losses. Conventional high-efficiency electric machines which use rare-earth permanent magnets (PM) are expensive, have thermal limitations and subject to availability concerns thereby deterring the sustainable development of EVs [2].

Machines that employ reluctance-type rotors have therefore become a topic of interest as alternatives that seek to eliminate the need for rare earth magnets and its associated challenges [3]. Reluctance-type outer-rotor topologies enable smooth and stable operation by dampening torque ripple due to the increased torque capability and benefits from opportunities for advanced cooling applied to the inner-stator housing majority of the active excitation [4].

The proposed novel design employs an outer rotor with an inner stator having spoke-type arrangement of non-rare earth magnets for flux intensification to reach high power density, eliminating the need for rare-earth PMs and overcoming the mechanical constraints of conventional outer stator designs [5]. The limitation imposed by outer stator designs on the depth of stator toroidal coils and PM height in the radial direction is eliminated as both can be geometrically extended along the rotor radius to increase effective coil and PM area without affecting rotor geometry. The capability to increase coil and PM area while maintaining a large rotor diameter allows for greater average torque and power density values as compared to inner rotor designs.

The computational model reviewed in this paper has been validated and compared with an experimental prototype of a high power density motor employing flux intensification techniques shown in Fig.1 [4]. The outer-rotor machine proposed, simulated, and optimized for electric vehicle applications provides a competitive alternative to rare-earth PM motors while delivering comparable performance in terms of goodness and efficiency.

II. Topology and Principle of Operation of the Proposed Electric Motor

The proposed outer-rotor configuration shown in Fig. 2 intensifies flux, operates through reluctance principles and is a variant of a previously investigated topology [4] [6]. A modular inner stator with sections containing PMs and concentrated coils per phase, intended for rectangular slots and

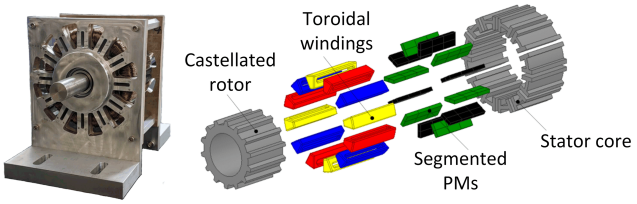

Fig. 1. Prototype and exploded view of existing high power density motor using a PM free castellated inner rotor and a modular stator with concentrated toroidal coils and tangentially magnetized PMs.

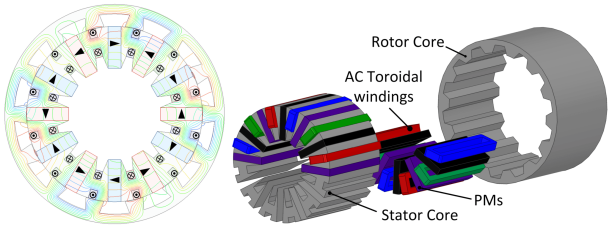

Fig. 2. Cross-sectional and exploded views of the proposed outer rotor ferrite motor with inner stator with concentrated toroidal coils and tangentially magnetized PMs for flux intensification on a 10in outer rotor diameter with a target torque of 360Nm at a base speed of 3,000rpm.

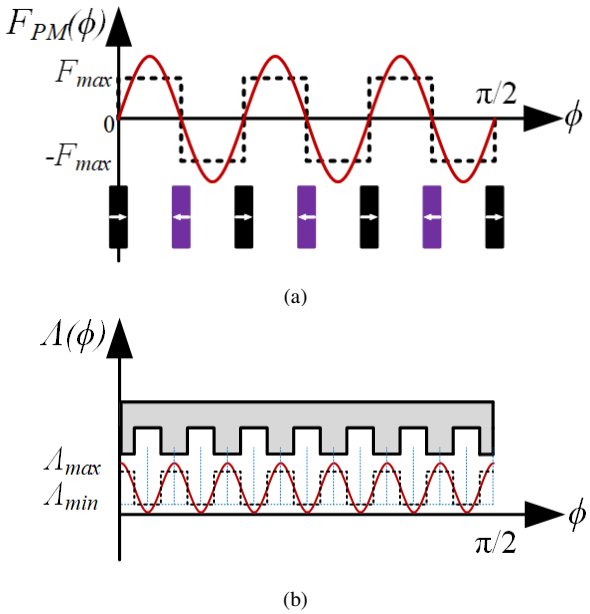

Fig. 4. Schematic of an MMF-permeance model for the proposed motor with (a) PM only, and (b) and with armature windings and airgap permeance (Λ).

wire to maximize fill factor [7]. The coils are toroidally wound with phases in succession around the stator circumference and have compact axial end portions. PMs are placed radially in the stator with consecutive PMs being tangentially magnetized in opposite directions. the PM length along the radius can be used to concentrate flux and achieve high airgap flux densities compared to its own remenance [8].

The reluctance-type laminated steel core rotor does not contain active excitation components and has protrusions which are coordinated with the characteristics of the stator. The movement of active excitation components to the inner-stator enables the application of advanced cooling techniques to mitigate thermal-based losses.

Torque is generated by the interaction of the PM field and armature windings produced by sets of stator PMs, rotor protrusions, and stator windings. The studied minimal region of periodicity is illustrated in Fig. 3 within the proposed concept and has 7 rotor protrusions, operating in a motor

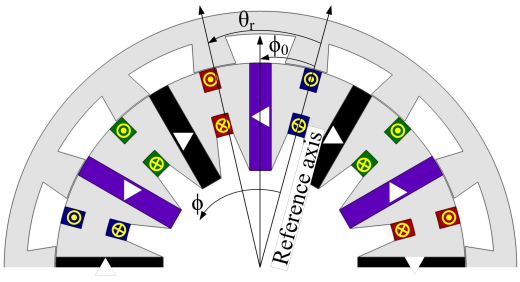

Fig. 3. Cross-section of a half periodicity region for the proposed motor design with 7 rotor protrusions. The noted angular coordinates as indicated are used in the analysis of the machine. The reference axis is middle of the stator slots.

with an equivalent of 14 magnetic poles. This region was repeated twice to produce 28 magnetic poles. To explain the working principle of the proposed motor concept and the torque generation mechanism, the open-circuit (OC) PM field and the armature field are analyzed using the MMF-permeance model depicted in Fig. 4 [4] [8].

To study the OC PM field, the armature windings are not considered, leaving only the PMs as the source of the magnetic field [4]. Without taking into account the stator slotting effect, the airgap flux density distribution produced by PMs can be calculated with [4]:

$$\begin{aligned} &B_{PM}(\varphi,t) = \\ &F_{PM}P_{PM}\frac{\Lambda_{avg}}{\kappa_{PM}}\ \sin\left(\kappa_{PM}\left(\phi-\phi_0\right)\right)+ \\ &F_{PM}P_{PM}\frac{\Lambda_{pp}}{4\kappa_{PM}}\sin\left(\kappa_{PM}+N_{pr}\right)\cdot \\ &\left[\phi-\frac{N_{pr}\omega_r t-\kappa_{PM}\phi_0-N_{pr}\theta_r}{\kappa_{PM}+N_{pr}}\right]+ \\ &F_{PM}P_{PM}\frac{\Lambda_{pp}}{\kappa_{PM}}\sin\left(\kappa_{PM}-N_{pr}\right)\cdot \\ &\left[\phi+\frac{N_{pr}\omega_r t+\kappa_{PM}\phi_0-N_{pr}\theta_r}{\kappa_{PM}-N_{pr}}\right], \end{aligned} \tag{1}$$

where, $B_{PM}(\phi,t)$ is the flux density distribution in the airgap due to PMs; F_{PM} the amplitude of the square-wave MMF created by PMs; Λ_{avg} the average of the maximum and minimum of the airgap permeance; Λ_{pp} the quarter of the difference between the maximum and minimum of the airgap permeance; P_{PM} half of the number of PMs; ϕ the mechanical angle alongside the peripheral of the airgap with its initial position with respect to the reference axis ϕ_0; κ_{PM} is equal to $(2k+1)P_{PM}$ and k is a positive integer; N_{pr}

the number of rotor protrusions, ω_r the mechanical speed of the rotor, and θ_r and t are the rotor initial position and time, respectively. Considering only the PMs as the source of magnetic flux, according to (1), there are three groups of flux density harmonics with different rotational speeds and respective pole pairs of κ_{PM}, $\kappa_{PM}+N_{pr}$ and $|\kappa_{PM}-N_{pr}|$.

The distribution of airgap flux density considering only the armature winding and neglecting PM contributions $B_{AR}(\phi,t)$ can also be similarly obtained as [4]:

$$\begin{aligned} B_{AR}(\varphi,t) &= \left(\frac{3}{\pi}\right) W_{max} I_m \Lambda_{avg} \cdot \\ &\sum_{m}^{\infty} \left(\frac{P_{AR}}{m}\right) \sin m \left[\phi - \phi_{a0} - \left(\frac{\omega t - \phi_a}{m}\right)\right] + \\ &\left(\frac{3}{4\pi}\right) W_{max} I_m \Lambda_{pp} \sum_{m}^{\infty} \left(\frac{P_{AR}}{m}\right) \sin\left(m + N_{pr}\right) \cdot \\ &\left[\phi - \frac{\omega t + \varphi_a - m\phi_{a0} - \left(N_{pr}\omega_r\right)(t+1)}{m + N_{pr}}\right] + \\ &\left(\frac{3}{4\pi}\right) W_{max} I_m \Lambda_{pp} \sum_{m}^{\infty} \left(\frac{P_{AR}}{m}\right) \sin\left(m - N_{pr}\right) \cdot \\ &\left[\phi - \frac{\omega t + \varphi_a - m\phi_{a0} + \left(N_{pr}\omega_r\right)(t+1)}{m - N_{pr}}\right], \end{aligned} \tag{2}$$

where, $B_{AR}(\phi,t)$ is the distribution of airgap flux density resulting solely from the armature windings; W_{max} and I_m are the peak values of saw-tooth wave winding function and phase current respectively; P_{AR} is the number of coils per phase in the armature winding; variables m, r, and t are positive integers, and $m = 3r+1 = tP_{AR}$; ω is the electrical frequency; ϕ_a the phase angle relative to ϕ_{a0} from the reference axis to the winding axis with three groups of flux density harmonics with m, $m+N_{pr}$, and $|m-N_{pr}|$ pole pairs.

Adjacent PMs are magnetized in the opposite direction of one another, which is illustrated in Fig. 4(a) providing flux intensification. The overall electromagnetic performance of the machine is determined by the combination of stator PMs, rotor protrusions and stator toroidal coils layout. The electromagnetic torque can be obtained using the principle of virtual work with the closed-form analytical airgap flux density distributions of PMs, $B_{PM}(\phi,t)$, and armature windings, $B_{AR}(\phi,t)$, and can be expressed by:

$$\begin{aligned} T_{emg} &= \frac{\partial W_{co}}{\partial \theta_r} = \frac{\partial}{\partial \theta_r} \int_V \frac{B(\phi,t)^2}{2\mu_0} \mathrm{d}V \\ &= \frac{D_s g \ell_{stk}}{4\mu_0} \frac{\partial}{\partial \theta_r} \int_0^{2\pi} \left[B_{PM}(\phi,t) + B_{AR}(\phi,t)\right]^2 \mathrm{d}\phi, \end{aligned} \tag{3}$$

where, D_s is the stator outer diameter, g the airgap length, and ℓ_{stk} the machine axial stack length. By using the orthogonal properties of sinusoidal behavior, it is inferred that a non-zero average electromagnetic torque can only be created by the interaction of the dominant airgap flux density harmonics from the PM and armature fields with pole pairs of 4, 6, 8, 16, 18, and 28 in the example motor.

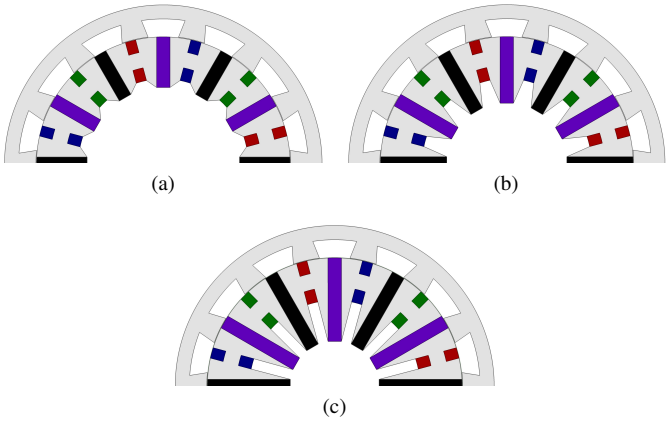

Fig. 5. Models of proposed motor design considering flux concentration ratios of (a) 1.5, (b) 2.0, and (c) 2.5.

The suitable combinations of stator PMs, rotor protrusions, and stator winding patterns that provide non-zero average torque can be derived by analyzing (3). The designs with 5, and 7 protrusions with a stator including 6 PMs and 6 toroidal coils, and the designs with 10, and 14 and seven protrusions with a stator including 12 PMs and 12 toroidal coils, are typical topologies produced from this method. The proposed topology explored herein has 14 rotor protrusions and 12 stator PMs and toroidal coils, that are a set of the possible working combinations of rotor protrusions, stator PMs and coils, which must be multiples of 5 or 7 and 6, respectively.

III. Design Considerations and Multi-Objective Optimization

In machines employing flux intensifying stators and reluctance rotors, a correlation has been found between the rotor geometry, torque, power density, and efficiency [4] [9] [10]. Parametric studies carried out for the choice of a 10 protrusions (20-P) or a 14 protrusions (28-P) rotor design show that the 14 protrusion machine has greater average torque, higher torque constant and power density as well as better efficiency compared to the 10 protrusion design. Reduction in anticipated torque ripple has also been found by increasing the number of rotor poles [11]. For a spoke-type PM arrangement as in the proposed topology, the airgap flux density can be expressed as:

$$B_{ag} = B_r \left(\frac{\pi D_g}{4 k_\sigma p h_{PM}} + \frac{2\mu_r g}{\ell_{PM}}\right)^{-1}, \tag{4}$$

where, D_g is the airgap diameter, p the number of pole pairs, μ_r the PM relative permeability, B_r the PM remanent flux density, and k_σ the rotor leakage coefficient, which can be adjusted to account for the saturation and slotting effects; the PM length in the direction of magnetization is ℓ_{PM} and the PM height along the rotor radius is h_{PM}. The airgap flux density varies directly with the PM remanent flux density, its length and height and for fixed values of PM length and height. The outer rotor design has the advantage of providing

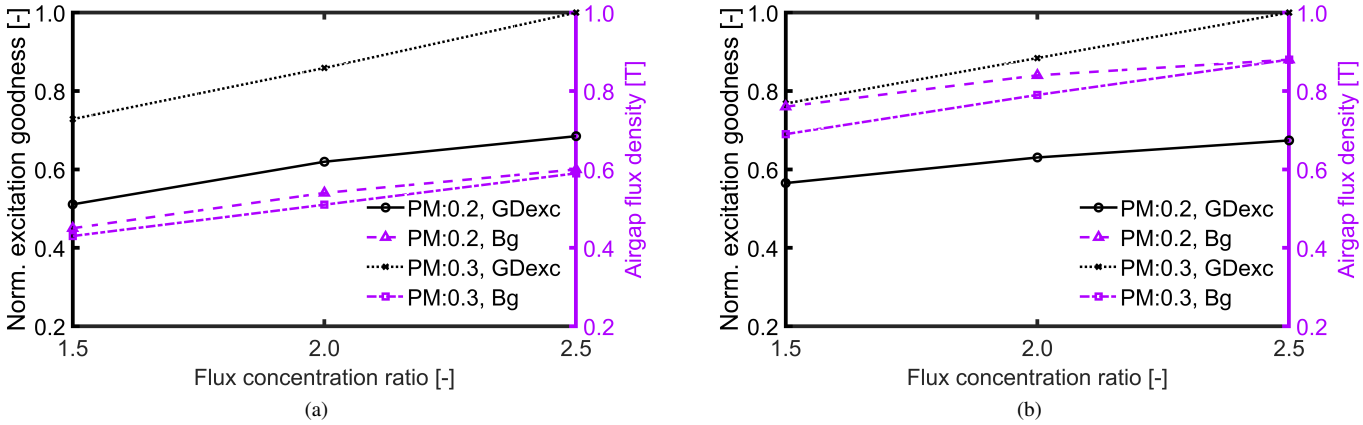

Fig. 6. Excitation goodness and absolute average airgap flux density at open-circuit for different ratios of PM width in the magnetization direction to stator pole pitch (as shown in the legend by PM:0.2, and PM:0.3) and different flux concentration ratios for ferrite with remanent flux density of (a) 0.4T and, (b) 0.8T

more space for the rotor pole height in the radial direction which increases the torque produced and hence overall motor performance.

Considering the length of the PM, a flux concentration ratio ξ can then be defined as the ratio

$$\xi = \frac{2h_{PM}}{\tau_p}, \tag{5}$$

where, τ_p is the stator pole pitch, i.e., stator outer circumference πD_s divided by the number of PMs n_{PM}. The flux concentration effect due to the spoke type arrangement employed in the proposed design is particularly beneficial for high polarity machines as the magnetic flux of two magnets contribute to the airgap magnetic flux in each pole [12]. Models wit flux concentration ratios of 1.5, 2.0 and 2.5 are shown in Fig. 5 amongst a wide range of achievable ratios. To determine optimal flux concentration ratio, a "excitation goodness" GD_{exc} is defined as

$$GD_{exc} = \frac{h_{PM} B_{PM} \ell_{stk}}{M_{PM}}, \tag{6}$$

where ℓ_{stk} is the motor stack length, B_{PM} and M_{PM} are the average flux density and mass for each PM respectively as calculated using 2D electromagnetic FEA employing the ANSYS Electronics Desktop software [13] [14], suitable ratios are found for the the PM length in the direction of magnetization l_{PM} and the PM height along the rotor radius h_{PM}. The airgap flux density and excitation goodness versus flux concentration ratio for the PMs with a remanent flux density of 0.4T and 0.8T are shown in Fig. 6, where, the base values for excitation goodness are equal to 0.92mWb/kg and 1.38mWb/kg respectively. The airgap flux concentration, PM weight, and flux concentration ratio increase with improvements to excitation goodness.

To determine a suitable flux concentration ratio, another metric of performance is introduced known as the machine goodness GD which is defined as

$$GD = \frac{T_{emg}}{\sqrt{P_{loss}}}, \tag{7}$$

where T_{emg} is the electromagnetic torque and P_{loss} is the total motor losses. The total loss P_{loss} in this motor is comprised of components in the laminated core, and winding copper, calculated as

$$\begin{aligned} P_{loss} &= P_{Cu} + P_{edy} + P_{Fe} \\ &= 3R_{ph}I_{ph}^2 + P_{edy} + \sum \left[P_h\left(B, f\right) + P_e\left(B, f^2\right) \right], \end{aligned} \tag{8}$$

where, the winding resistance and current per phase are R_{ph}, and I_{ph}, respectively and P_{edy} the eddy current losses in the winding. Core losses include hysteresis P_h and eddy current losses P_e, both as a function of frequency f and magnetic flux density B. The flux concentration and PM width to stator pole pitch ratios have been found to have negligible influence on the copper losses as constant electrical loading is assumed in the analysis. Winding supplementary eddy current losses P_{edy} have been neglected for the purpose of this study. For the proposed motor concept, the machine goodness at different flux concentration, and PM width to stator pole pitch ratios, is as in Fig. 7a for PM remanent flux densities of 0.4T and 0.8T. A flux concentration of 2 with PM width ratio of 0.3 is considered an optimal choice for the proposed motor topology.

Multi-objective optimization employing FEA and differential evolution targeting maximization of ratio of average torque to stack length T_e/L, minimization of total machine loss P_{loss}, and minimization of torque ripple T_{rip} while exceeding a minimum power factor pf constraint was performed [13]. Various geometric ratios that bound the optimization (such as ratio of outer to inner rotor diameter, airgap length, AC slot width and depth etc.) were selected within investigated limits that would yield robust and mechanically stable designs meeting said optimization objectives.

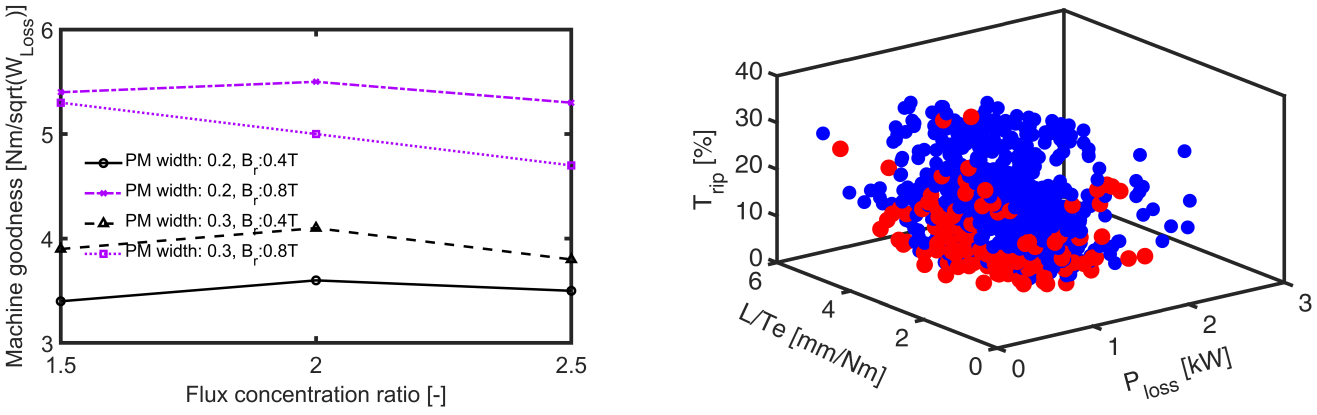

(a) (b)

Fig. 7. (a)Machine goodness for flux concentrations of 1.5 to 2.5 and for two different values of PM width ratio to stator pole pitch, and (b) optimization results: 3D pareto front projection with objectives of stack length to average torque, total loss, and torque ripple.

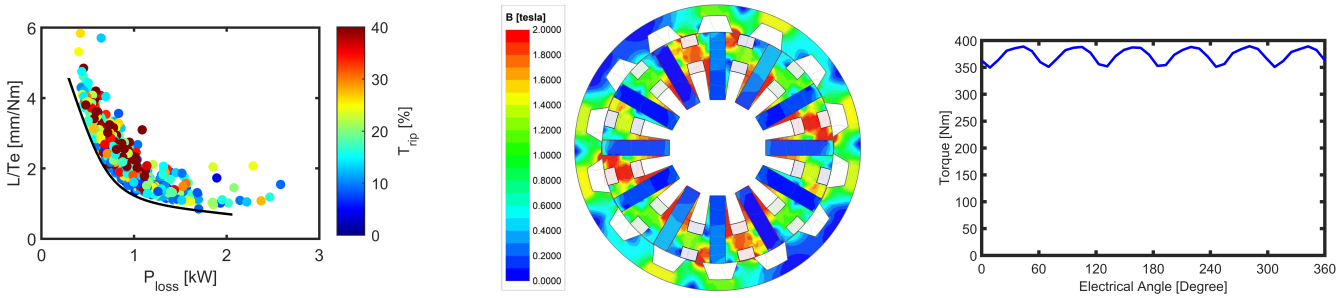

(a) (b) (c)

Fig. 8. (a) Optimization results projected for torque - total loss plane showing torque ripple variation , (b) cross-sectional view of the selected "best" design OR-PM D1 with a plot of the flux density and lines, and (c) torque waveform of selected "best' design OR-PM D1.

IV. Results and Discussion

The 3D Pareto of the optimization results shows that the best designs represented by red dots have the highest values of torque per stack length, lowest values of torque ripple and total losses as shown in Fig. 7b. Projection of the optimization results unto the torque-total loss plane in Fig. 8a shows that no one design has the best of all desired optimization objectives and a compromise has to be made in final selection. Table I gives the performance summary of the selected "best" design OR-PM D1 while its cross-section overlayed with its flux density plot and flux lines is as shown in Fig. 8b. For a peak torque of 373Nm, the selected design has a specific torque constant k_T of 12.1Nm/(A/mm^2).

$$k_T = \frac{T_{emg}}{J}, \tag{9}$$

where, J is the copper current density of the winding. The torque ripple is approximately 10% as in Fig. 8c which may be considered satisfactory for typical applications and can be further improved through optimization.

A comparison of the selected "best" design OR-PM D1 with commercially available high power density traction motors considering their approximate performances based on publicly available information is as given in Table II shows competitive performance with these commercially available state-of-art motors [15].

TABLE I
Performance Specifications for OR-PM D1

Peak Torque [Nm]	373
Continuous Torque [Nm]	191
Max. power [kW]	117
Base speed [rpm]	3,000
Max. speed [rpm]	14,400
Rotor OD [mm]	255
Stack length [mm]	150
Total active mass [kg]	38

The efficiency map at room temperature for the selected "best" design OR-PM D1 for the proposed outer rotor design is shown in Fig. 9 dicates capability for high efficiency operation even at the maximum considered speed. The motor can be seen to have its highest efficiency in the region of its continuous torque.

V. Conclusion

A special outer-rotor electric machine topology was proposed, simulated, and optimized for electric vehicle traction

TABLE II
PERFORMANCE COMPARISON WITH HIGH POWER DENSITY TRACTION MOTORS

	Type	Peak Torque [Nm]	Active Mass [kg]	TRW [Nm/kg]
OR-PM D1	New	373	38	9.8
Honda Accord 14	IPM (V)	306	33	9.3
YASA 400	Axial PM	360	24	15.0
Toyota Prius 10	IPM (V)	207	23	9.0
Chevrolet Bolt EV	IPM (V)	360	33	10.9
Tesla S	Induction	430	55	7.8

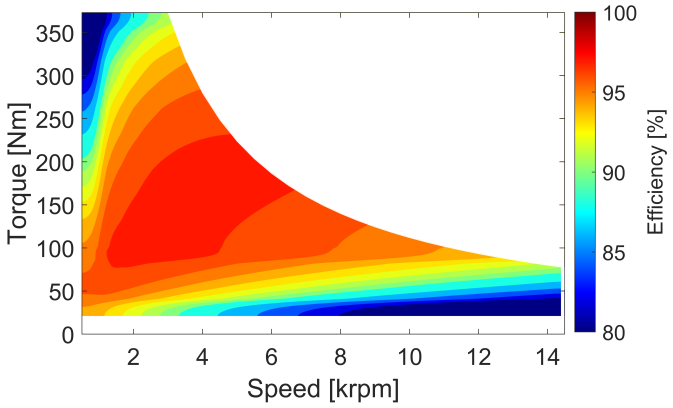

Fig. 9. Efficiency map of OR-PM D1 showing its performance in constant torque and constant power regions. Best performance occurs around the base speed and in the continuous torque regions.

applications. The outer rotor design eliminates the mechanical limitations imposed by an outer stator design allowing for a geometrically larger rotor, increased effective coil and PM area through extension of stator toroidal coil depth and PM height in the radial direction resulting in greater average torque and power density values. Most of the losses in the proposed motor are localized to the stator therefore highly efficient cooling arrangements can be employed.

The flux focusing effect enables potential reduction in ferrite utilization at a comparable performance to other non-rare earth variants with a higher remanence. The optimized resulting model has comparable goodness to existing alternatives using rare-earth magnetic materials and its comparison with other state-of-the art high power density motors shows competitive performance. The efficiency map of the selected "best" design shows that the motor is capable of high efficiency operation, especially at its continuous torque region. With flux weakening, the targeted design is capability of operation at high speeds, providing an extended constant power region with thermal and demagnetization.

ACKNOWLEDGMENT

The support of QM Power, Inc., Ansys Inc., and University of Kentucky, the L. Stanley Pigman Chair in Power endowment is gratefully acknowledged.

REFERENCES

[1] I. Husain, B. Ozpineci, M. S. Islam, E. Gurpinar, G.-J. Su, W. Yu, S. Chowdhury, L. Xue, D. Rahman, and R. Sahu, "Electric drive technology trends, challenges, and opportunities for future electric vehicles," *Proceedings of the IEEE*, vol. 109, no. 6, pp. 1039–1059, 2021.

[2] B. Sarlioglu, C. T. Morris, D. Han, and S. Li, "Driving toward accessibility: a review of technological improvements for electric machines, power electronics, and batteries for electric and hybrid vehicles," *IEEE Industry Applications Magazine*, vol. 23, no. 1, pp. 14–25, 2016.

[3] M. Obata, S. Morimoto, M. Sanada, and Y. Inoue, "Performance of pmasynrm with ferrite magnets for ev/hev applications considering productivity," *IEEE Transactions on Industry Applications*, vol. 50, no. 4, pp. 2427–2435, 2014.

[4] P. Han, M. G. Kesgin, D. M. Ionel, R. Gosalia, N. Shah, C. J. Flynn, C. S. Goli, S. Essakiappan, and M. Manjrekar, "Design optimization of a very high power density motor with a reluctance rotor and a modular stator having pms and toroidal windings," in *2021 IEEE Energy Conversion Congress and Exposition (ECCE)*. IEEE, 2021, pp. 4424–4430.

[5] A. Mohammadi and S. M. Mirimani, "Design of a novel pm-assisted synchronous reluctance motor topology using v-shape permanent magnets for improvement of torque characteristic," *IEEE Transactions on Energy Conversion*, vol. 37, no. 1, pp. 424–432, 2022.

[6] D. M. Ionel, J. Eastham, and T. Betzer, "Finite element analysis of a novel brushless dc motor with flux barriers," *IEEE Transactions on magnetics*, vol. 31, no. 6, pp. 3749–3751, 1995.

[7] G. Heins, D. M. Ionel, and M. Thiele, "Winding factors and magnetic fields in permanent-magnet brushless machines with concentrated windings and modular stator cores," *IEEE Transactions on Industry Applications*, vol. 51, no. 4, pp. 2924–2932, 2015.

[8] A. Mohammadi, O. A. Badewa, Y. Chulaee, D. M. Ionel, S. Essakiappan, and M. Manjrekar, "Direct-drive wind generator concept with non-rare-earth pm flux intensifying stator and reluctance outer rotor," in *2022 11th International Conference on Renewable Energy Research and Application (ICRERA)*. IEEE, 2022, pp. 582–587.

[9] S. M. Castano, R. Yang, C. Mak, B. Bilgin, and A. Emadi, "External-rotor switched reluctance motor for direct-drive home appliances," in *IECON 2018-44th Annual Conference of the IEEE Industrial Electronics Society*. IEEE, 2018, pp. 514–521.

[10] B. Anvari, H. A. Toliyat, and B. Fahimi, "Simultaneous optimization of geometry and firing angles for in-wheel switched reluctance motor drive," *IEEE Transactions on Transportation Electrification*, vol. 4, no. 1, pp. 322–329, 2017.

[11] S. Singh, H. V. Singh, C. Shivshankar, A. Gupta, A. Shakya, D. Tripathi, and A. Kumar, "Design and simulation of 4 kw, 12/8 switched reluctance motor for electric three-wheeler," *Materials Today: Proceedings*, vol. 65, pp. 3461–3475, 2022.

[12] D. M. Ionel, D. Jackson, G. Starr, and A. Turner, "Permanent magnet brushless motors for industrial variable speed drives," in *2002 International Conference on Power Electronics, Machines and Drives (Conf. Publ. No. 487)*. IET, 2002, pp. 650–654.

[13] M. Rosu, P. Zhou, D. Lin, D. M. Ionel, M. Popescu, F. Blaabjerg, V. Rallabandi, and D. Staton, *Multiphysics simulation by design for electrical machines, power electronics and drives*. John Wiley & Sons, 2017.

[14] *Ansys® Electronics, version 21.2, 2021, ANSYS Inc.*

[15] A. Fatemi, D. M. Ionel, M. Popescu, Y. C. Chong, and N. A. Demerdash, "Design optimization of a high torque density spoke-type pm motor for a formula e race drive cycle," *IEEE Transactions on Industry Applications*, vol. 54, no. 5, pp. 4343–4354, 2018.